Scaling properties for the surfaces of fractal and nonfractal objects: An infinite hierarchy of critical exponents

Paul Meakin,* Antonio Coniglio,† and H. Eugene Stanley

Center for Polymer Studies and Department of Physics, Boston University, Boston, Massachusetts 02215

Thomas A. Witten

Corporate Research Science Laboratories, Exxon Research and Engineering Company, Annandale, New Jersey 08801
(Received 25 April 1986)

A recent finding of Meakin et al. and Halsey et al. is that the surface of diffusion-limited aggregates (DLA) requires an infinite hierarchy of fractal dimensions for its characterization. In this work, we seek to understand this discovery and to place it into perspective. To this end, we study the distribution of hit probabilities near the surface of a variety of suitably chosen fractal and nonfractal objects—ranging from DLA and screened-growth aggregates on the one hand to simple A-arm stars and S-sided polygons on the other. We show physically how the infinite hierarchy of fractal dimensions arises, even for nonfractal objects. An important difference however, is that the infinite hierarchy is characterized by a constant gap exponent for the nonfractal objects, while for DLA a constant gap exponent is not sufficient.

I. INTRODUCTION

A fractal object such as a polymer in solution or a colloidal aggregate exhibits remarkably strong screening behavior. As these objects are made larger, their density becomes indefinitely small, yet their interior is progressively better screened from external fields. Thus, e.g., a polymer of radius of gyration R behaves hydrodynamically like a dense sphere with a comparable radius. External flow does not penetrate into the interior, and only a small part of the polymer experiences the external flow. Analogous screening occurs when the fractal is an electrical conductor or when it is an absorbing sink for some diffusing substance. Thus the screening properties of a fractal have an important bearing on their special rheological, electrical, and catalytic properties. It is thus of interest to examine how screening occurs by characterizing the subset of the structure responsible for the screening.

The idea that a specific part of a fractal is responsible for its screening provides one concept of a "surface" for the fractal. The broader question of how to characterize the surface of complex structures is important for their adsorption, optical, and acoustic properties, as well as those listed above. Many of these properties may be expressed in terms of the interaction of the structure with probe particles, which come from the exterior of the object and move according to some physical law.

This paper is a sequel to two papers[1,2] which address the question of how to characterize the surface of a fractal object.[3] The first paper[1] recognized the fact that only a minute fraction of the total surface sites is responsible for the screening, and developed a mean-field theory for this fraction of "unscreened" sites. The second paper[2] tested this mean-field theory by first introducing the basic variable p, the probability that a site i is the next to be hit and then calculating the hit distribution function $N(p)$.

Here $N(p)\Delta p$ is the number of perimeter sites for which p is in the range $(p, p + \Delta p)$. Reference 2 found the mean-field theory of Ref. 1 to be reasonably accurate when low moments of $N(p)$ were considered, but not so accurate for high moments. The high moments weight the most exposed "hottest" tips of the fractal the heaviest, and it was found that not only did the high moments scale differently than the low moments but successive high moments did not scale in the same fashion. Thus, instead of a single exponent being sufficient to describe the critical behavior of $N(p)$, one needs an entire hierarchy of exponents.[2,4–8]

The purpose of this paper is to explore the physical basis and implications of this discovery of an infinite hierarchy of scaling exponents, with a view toward developing some understanding of the surface of a fractal object. To this end, we consider the anomalous behavior found even for certain nonfractal objects, such as simple S-arm star structures and needles, and also S-sided polygons. We also attempt to answer the important question of when one should expect to find an infinite hierarchy of exponents by making comparison with recent work on the voltage distribution across the bonds of a percolation cluster.[5]

In Sec. II we develop further the mean-field theory of Ref. 1, which predicts that a single exponent is sufficient to describe the unscreened surface of a fractal object. In Sec. III we consider the modification of mean-field theory needed when very large moments of $N(p)$ are considered, while in Sec. IV we consider the scaling behavior of general moments. Section V describes computer models, and Sec. VI applies this first to needles and A-arm stars and then—in Sec. VII—to S-sided polygons. Section VIII is an extensive discussion of the surface of a DLA (diffusion-limited aggregation) cluster[9,10] while Sec. IX concerns a family of screened growth aggregates[11–13] for which the fractal dimension can be tuned at will.

II. MEAN-FIELD THEORY

The definition of the "surface" of an irregular ramified object, such as a biological macromolecule or cross-linked gel, is a question of great current interest that was addressed recently by Coniglio and Stanley (CS).[1] They noted the distinction between the geometric surface of an object and the vanishingly small subset of that surface that can actually be reached by some probe. Consider, for example, a macromolecule. Naively, one expects that the total surface area doubles when the mass doubles. A large portion of the surface is so well "screened" by the outer part of the macromolecule that the part of the surface which is "unscreened" is vastly smaller than the total surface. Moreover, this unscreened surface scales totally differently than the total surface: If the total surface is doubled, the unscreened portion increases by a factor smaller than 2. This consideration seems at first sight academic, but when we recall that many biological macromolecules are triggered by the arrival of diffusing particles, we realize that the properties of this unscreened perimeter are responsible for controlling fundamental biological processes.

To make these concepts quantitative, CS formulated a simple mean-field treatment of the unscreened perimeter of a fractal object [Fig. 1(a)]. They found that M_u, the number (or "mass") of unscreened surface sites, scales with the molecular diameter L as

$$M_u \sim L^{d_u} , \tag{2.1}$$

with

$$d_u = (D-1) + (d-D)/d_p . \tag{2.2}$$

Here d_u is the fractal dimension of the unscreened perimeter, D is the fractal dimension of the cluster or "macromolecule," and d_p is the fractal dimension of the walk taken by the incoming particles (e.g., $d_p = 2$ for a diffusing particle and $d_p = 1$ for linear trajectories). A similar result was also found by Meakin and Witten[14] for the interface of DLA clusters.

Equation (2.2) has a simple physical interpretation [Fig.

1(b)]. The first term in parentheses corresponds to the "cookie-cutter perimeter" (which is found if we simply cut the fractal) whose length scales as L^{D-1}. The second term corresponds to the fact that walks with noninfinite fractal dimension will penetrate the fractal to a mean depth $\lambda \sim L^{(d-D)/d_p}$. It is physically plausible that the degree of penetration is controlled by the co-dimension of the fractal, $(d-D)$, and by the fractal dimension of the walk, d_p.

Equation (2.2) was put to a direct test by an extensive series of numerical calculations by Meakin, Stanley, Coniglio, and Witten (MSCW).[2] Specifically, MSCW calculated the "hit probability," p_i, the probability that perimeter site i is the next to be hit. This was done by first fixing a large DLA cluster [Fig. 2(a)], and then sending typically 10^6 random walkers at the cluster. Counters on each perimeter site record how many times that perimeter site is hit. Figures 2(a)–2(d) show the actual MCSW results. If the mean-field theory were completely correct, then the "hit distribution" of Figs. 2(b)–2(d) would be quite different: the hits would be more or less concentrated [like Fig. 1(b)] in a band of width λ, and the band would not change much from Fig. 2(b) to Fig. 2(d).

To quantitatively analyze the phenomenon of Figs. 2(b)–2(d), MCSW introduced the family of moments

$$Z_q \equiv \sum_{i=1}^{M} p_i^q , \tag{2.3}$$

where M is the total number of sites. The mean-field ansatz is then the statement that

$$p_i = \begin{cases} \bar{p} , & i = 1, 2, \ldots, M_u \\ 0 , & \text{otherwise} . \end{cases} \tag{2.4}$$

Hence the qth moment is given by

$$Z_q = [(\bar{p})^q M_u] . \tag{2.5}$$

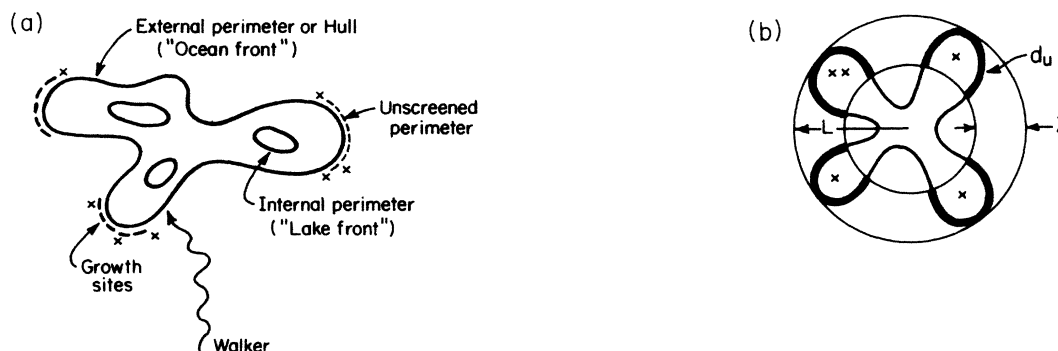Now $\bar{p}$ is fixed by the normalization condition

FIG. 1. (a) Schematic illustration of different fractal surfaces arising in the description of a general cluster. (i) The external perimeter or hull has a fractal dimension d_h. (ii) The total perimeter has a fractal dimension D, equal to that of the total bulk mass of the cluster. Since $D > d_h$, it follows that the internal perimeter must have the same fractal dimension D as the total perimeter. (iii) The unscreened perimeter where an incoming walker is more likely to hit has a fractal dimension d_u. (b) Schematic illustration of parameters needed to obtain the mean-field expression, Eq. (2.2), for the fractal dimension of the unscreened perimeter. The symbol $\times$ denotes a typical cluster site that is hit by an incoming random walk, while λ is the mean thickness of this band of sites.

$$\sum_{i=1}^{M} p_i = \sum_{i=1}^{M_u} \bar{p} = 1 \ . \tag{2.6}$$

From (2.6) it follows that

$$\bar{p} = 1/M_u \ . \tag{2.7}$$

Substituting (2.7) into (2.5), we find that in the mean-field limit the scaling of $Z_q^{-1/(q-1)}$ is independent of q, with

$$Z_q = M_u^{-(q-1)} \sim L^{-(q-1)d_u} \ . \tag{2.8}$$

When MSCW calculated Z_q for small q, their results were consistent with the mean-field prediction. Thus the CS mean-field theory provides a good description of physical phenomena that depend on low moments, such as electrical conductivity[1] in a random superconducting network. This is why the predictions of Ref. 1 for the conductivity problem are in good agreement with numerical results.

However, when MSCW considered much larger values of q, they found systematic deviations from the mean-

field value (Fig. 3), as we shall now discuss.

For q sufficiently large, we would surely expect the CS mean-field result (2.8) to fail: since only the most exposed tips of the DLA perimeter are favored in the moment sum (2.3), we would expect λ to have a q-dependent exponent, not the q-independent exponent $(d-D)/d_p$ of Ref. 1. In fact, MCSW found that for large values of q, (2.8) fails quite seriously (Fig. 3). Here we replace (2.8) by

$$Z_q \sim L^{-(q-1)D(q)} \ , \tag{2.9}$$

where $d_u = D(q)$ is now q dependent.

III. VERY HIGH MOMENTS: THE LARGE-q LIMIT

Note that the p values in the summand of (2.3) can be binned, and a distribution function $N(p)$ introduced, where $N(p)$ is the number of sites whose p values fall in the range $(p, p + \Delta p)$. Thus we can write

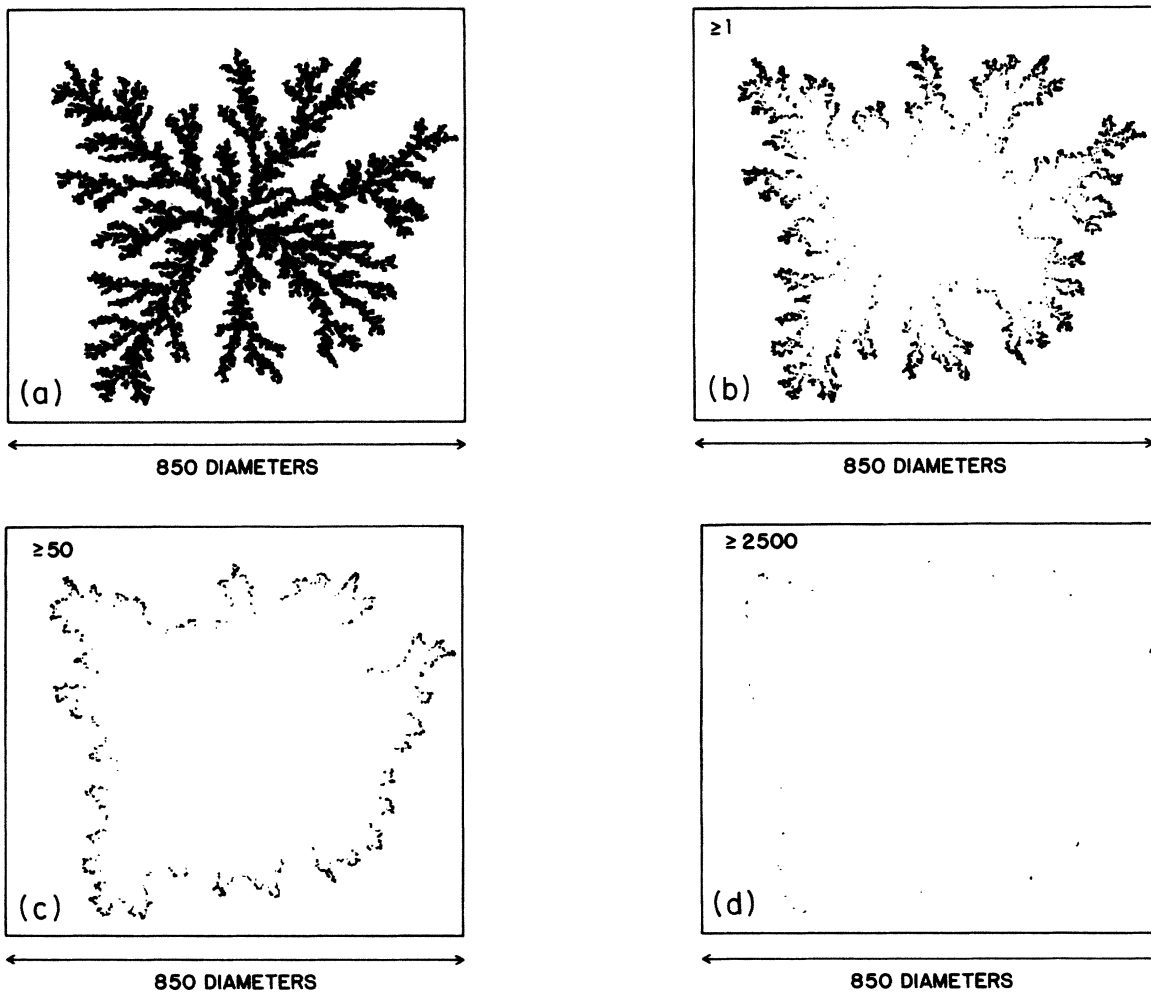$$Z_q = \sum_{p} N(p) p^q \ . \tag{3.1a}$$

FIG. 2. This figure illustrates the harmonic measure for a 50 000 particle off-lattice 2D DLA aggregate. (a) shows the cluster. (b) shows all 6803 particles which have been contacted by at least one of 10^6 random walkers (following off-lattice trajectories). (c) shows all of those particles which have been contacted 50 or more times and (d) shows those particles have been contacted 2500 or more times. The maximum number of contacts for any particle was 8197 so that $p_{max} = 8.2 \times 10^{-3}$.
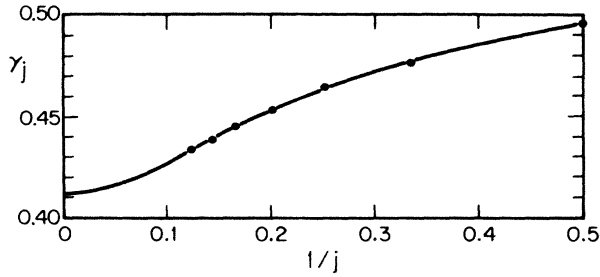
FIG. 3. The exponent $\gamma_j = D(q)/D$, where $q = j + 1$, which characterizes the behavior of the jth moment of p_i. Here p_i is the probability that perimeter site i is the next site at which the cluster will grow. For small j, γ_j is close to the mean-field value $\gamma_j = 1$, but for higher moments the γ_j approach the expected limit, $1 - 1/D$.

We will see that $\ln p$ is the natural variable in this problem, which motivates a logarithmic binning (such as $\frac{1}{2} < p < 1$, $\frac{1}{4} \leq p < \frac{1}{2}$, $\frac{1}{8} < p < \frac{1}{4}, \ldots$). Hence (3.1a) becomes

$$Z_q = \sum_{\ln p} n(p) p^q , \tag{3.1b}$$

where $n(p)$ is the number of sites for which $\ln p$ is in the range $(\ln p, \ln p + \Delta \ln p)$. In the limit of small Δp,

$$n(p) = p N(p) . \tag{3.1c}$$

We next note the following inequality:

$$Z_q \geq [(p_{max})^q n(p_{max})] . \tag{3.2a}$$

Here

$$p_{max} \sim L^{-\alpha_{max}} , \tag{3.2b}$$

is the maximum value of p, and

$$n(p_{max}) \sim L^{f_{max}} , \tag{3.2c}$$

is the fractal set of perimeter sites characterized by the value $p = p_{max}$. For q sufficiently large, the sum in (2.3) is dominated by the maximum value of p, and (3.2a) holds as an equality. Hence if we combine (3.2) with (2.9), we find

$$(q - 1)D(q) = q\alpha_{max} - f_{max} . \tag{3.3}$$

Note that (3.3) would reduce to the mean-field result (2.8) if $f_{max} = \alpha_{max} = d_u$. We discuss the generality of this behavior of $D(q)$ in Sec. V. Equation (3.3) was first obtained in Ref. 6, where α_{max} and f_{max} were believed to be independent of q (i.e., Z_q has a family of exponents, but with a constant "gap" α_{max}). We shall see that this assumption is overly restrictive.

IV. ARBITRARY MOMENTS: THE CASE OF GENERAL q

When q is not extremely large, the approximation described above breaks down except for special cases where $N(p)$ can be described by a power law in p (see Sec.

V). For general q, the sum in (2.3) is no longer dominated by p_{max}, but rather by some other value $p = p^*$, where in general

$$p^* = p^*(q) \tag{4.1}$$

depends on the value of q. This p^* is the value of p that maximizes the summand $n(p)p^q = \exp[\ln n(p) + q \ln p]$. It is the solution of the equation

$$\frac{d \ln n(p)}{d \ln p} = -q . \tag{4.2}$$

Let us define the new exponents $\alpha(q)$ and $f(q)$ by the analogs of (3.2a) and (3.2b),

$$p^*(q) \sim A(q) L^{-\alpha(q)} , \tag{4.3a}$$

and

$$n(p^*) \sim B(q) L^{f(q)} . \tag{4.3b}$$

Then

$$(q - 1)D(q) = q\alpha(q) - f(q) . \tag{4.4}$$

From (4.2) it follows that

$$\frac{d}{dq}[(q - 1)D(q)] = \alpha(q) . \tag{4.5}$$

Thus if we know $D(q)$, then $\alpha(q)$ follows from (4.5) and, finally, $f(q)$ from (4.4). A similar approach leading to (4.4) and (4.5) has been developed in Ref. 7.

We note that the normalization condition $\sum_{p^*} n(p^*) p^* = 1$ implies $\sum_q L^{f(q) - \alpha(q)} = 1$. Hence,

$$f(q) \leq \alpha(q) , \tag{4.6}$$

with the equal sign holding for $q = 1$.

Note also that $p^*(q) \rightarrow p_{max}$ as $q \rightarrow \infty$, so if we set $\alpha_{max} = \alpha(\infty)$,

$$p_{max} \sim L^{-\alpha(\infty)} . \tag{4.7}$$

From (4.7) and (4.2), we find that in the asymptotic large-L limit,

$$x \equiv \frac{\ln p^*}{\ln p_{max}} = \frac{\alpha(q)}{\alpha(\infty)} , \tag{4.8}$$

plus terms of order $(1/\ln L)$. Inverting (4.8), we have

$$q = q(x) . \tag{4.9}$$

Substituting in (4.3), we finally obtain

$$n(p) = C(x) L^{\phi(x)} , \tag{4.10}$$

where $x = \ln p / \ln p_{max}$, $C(x) = B[q(x)]$, and $\phi(x) = f[q(x)]$. Note that we have replaced p^* by p since p^* can be considered to be an independent variable. That is, (4.8) is a functional equation valid for all values of p^* and hence for all values of p.

Equation (4.10) gives the scaling behavior for the hit distribution function $n(p)$.[15] The actual exponent in (4.4) depends on the ratio $\ln p / \ln p_{max}$, which reduces to the usual scaling with only one scaling exponent when $\alpha(q)$ is independent of q. Similar scaling is also found for the

voltage distribution in a random resistor network, when p is replaced by the voltage across a bond in the backbone of a percolation cluster.[16]

V. SCALING OF $N(p)$ FOR NONUNIFORM ABSORBERS: POLYGONS, NEEDLES, AND STARS

In the previous discussion when the incoming probes are diffusive particles, the probability, $p(x)$, that a random walker hits the side x of the surface of the aggregate coincides with the distribution of diffusing flux on such a point. Since this probability can also be obtained by solving the Laplace equation with absorbing boundary conditions on the aggregate, it is also called the harmonic probability measure.

There is a special motivation for studying this diffusing flux for fractals like diffusion-limited aggregates (DLA), whose form is itself controlled by the properties of this flux. In DLA, particles are added one at a time to a growing cluster or aggregate of particles via random-walk trajectories, starting from randomly positioned distant points. If the particle reaches a position on the surface of the growing cluster of particles, it is added to the cluster at that position. The event which describes the growth process is the arrival of the particle at the surface. Thus the harmonic measure not only characterizes the surface of the cluster but also the growth process. For other growing objects, the measure is provided by the growth probability.

To define the distribution of flux onto an absorbing object, more generally, we suppose that the space around the object contains a "harmonic" field $u(r)$, satisfying $\nabla^2 u = 0$. This u may be heat, some molecular species, or momentum in a quiescent, viscous fluid. We take our object to be a perfect absorber of the field, so that $u = 0$ on the absorber. The flux $p(x)$ at some point x on this absorber is the rate at which diffusing particles are absorbed at x. For a smooth surface, it is the magnitude of ∇u at x; this gradient is always normal to the surface.

The distribution of hit probabilities can show interesting scaling behavior even when the object is not fractal. Such scaling behavior emerges for any object with sharp corners, such as a polygon or star. If the opening angle of a corner is γ, then the flux density $p(x)$ at distance x from the corner varies as $x^{-\beta}$, with $\beta = (1 - \gamma/\pi)/(2 - \gamma/\pi)$. The most singular case is a needle, where $\gamma = 0$ and $\beta = \frac{1}{2}$. The power-law behavior holds out to distances x of the order of the side length L of the polygon. For definiteness, we divide the absorbing object into a lattice of cells of size "a." Then we may normalize the flux $p(x)$ so that it gives the probability that a given diffusing particle lands at the cell at x, i.e., $\sum_x p(x) = 1$. For the weak singularities encountered here $(\beta < 1)$ the sum is dominated by the largest distances, of order L,

$$1 = \sum_x p(x) \simeq p(L)L . \tag{5.1}$$

Thus $p(L) \sim a/L$.

The exponents $D(q)$ may be readily calculated for such objects using the hit distribution $N(p)$ as defined above.

For the interval $a < x < L$ where $p(x) \sim x^{-\beta}$, $N(p) \sim p^{-1 - 1/\beta}$ for p, between some $p_0 = p(L)$ and $p_{max} = p(a)$. This is readily checked by using the definition of $N(p)$, namely, $N(p) = \sum_x \delta[p(x) - p]$.

The moments Z_q may be expressed in terms of p_0 and p_{max} using Eq. (3.1) and $N(p) \sim p^{-1 - 1/\beta}$. For small moments such that $q - 1/\beta < 0$, the integral is dominated by the smallest p's, of the order of p_0: $M_q^{-(q-1)} \sim p_0^{q-1} \int dp \, N(p) p$. The integral is unity because of our normalization. Thus

$$Z_q \sim p_0^{(q-1)} , \quad q < 1/\beta . \tag{5.2a}$$

It is convenient to introduce the function M_q defined by

$$M_q \equiv Z_q^{-1/(q-1)} \sim L^{D(q)} . \tag{5.2b}$$

Combining (5.2a) and (5.2b), we have $M_q \sim p_0^{-1}$. This scaling is independent of the moment taken.

For higher moments, the scaling becomes more complicated. If $q - 1/\beta > 0$ the largest p's dominate the integral,

$$M_q^{-(q-1)} \sim p_0^{(q-1)} \left[\frac{p_{max}}{p_0} \right]^{q - 1/\beta} . \tag{5.3}$$

Since p_0 and p_{max} scale differently with the size L of the polygon, the M_q must now scale differently for different q. Using $p_0 \sim 1/L$ and $p_{max}/p_0 \sim L^\beta$, and recalling that $M_q \sim L^{D(q)}$, we find

$$D(q) = \begin{cases} 1 + (\beta q - 1)/(q - 1) , & q > 1/\beta \\ 1 , & q < 1/\beta . \end{cases} \tag{5.4}$$

Thus for these nonfractal objects, the exponents $(q - 1)D(q)$ vary linearly with q, as was found in mean-field theory[1] and in some of the early calculations[6] for DLA, but the present discussion shows that different powers $D(q)$ may occur for quite ordinary objects, as noted recently in a different context.[7]

The derivation of (5.2) and (5.3) is valid whenever $N(p)$ has a power-law behavior in some range $p_0 < p < p_{max}$. The adsorber need not be a polygon. The power $-1 - 1/\beta$ must be more negative than -2; otherwise even the normalization integral is controlled by p_{max}, and all moments M_q scale as p_{max}^{-1}. One instructive extension is the case of a regular "asterisk" made of A radial needles of length L. The important region for all the positive moments M_q is the region near each needle tip: $x < L[1 - \cos(2\pi/A)]$. For the large-p values of this region, $\beta = \frac{1}{2}$ and $N(p) \sim p^{-3}$. The other asymptotic regime is the V-shaped regions near the center. The V angles are $2\pi/A$, so that the angle γ defined above is $2\pi(1 - 1/A)$, and $\beta = 1 - A/2$. For the p values found near the center, $N(p) \sim p^{(A-4)/(2-A)}$. Thus $N(p)$ consists of two power-law regimes, one for the most exposed regions, the other for the most protected regions. Only the exposed region proves to be important for calculating the positive moments of the flux distribution and the corresponding exponent $D(q)$.

Fractal objects, like the nonfractal ones discussed above, are expected to have a broad distribution $N(p)$ of flux intensities, and we may generalize the above discussion to include these. The range of p for an object of size

L extends from the p_{min} of the most protected point to the p_{max} of the most exposed point. Between these extremes lies the median, p_0, which we now define explicitly by

$$\int_{p_0}^{\infty} pN(p)dp = \tfrac{1}{2} \ . \qquad (5.5)$$

As with the asterisk discussed above, only the exposed or unscreened regime between p_0 and p_{max} is important for the non-negative moments. The complementary screened region $p_{min} < p < p_0$ may be large in the sense $p_0/p_{min} \gg p_{max}/p_0$. In a fractal (though not in an asterisk), the unscreened region may even become a vanishingly small part of the object, so that

$$\int_{p_0}^{\infty} N(p)/M \to 0 \ , \qquad (5.6)$$

where the number of elementary cells in the object, M, can be expressed as

$$M = \int_0^{\infty} N(p) \ . \qquad (5.7)$$

The scaling of the moments M_q with the mass M depends on the behavior of $N(p)$ between p_0 and p_{max}. In a simple smooth object, where p_{max}/p_0 remains bounded as $M \to \infty$, all the M_q scale as p_0^{-1}; this is the only scale available for expressing the M_q. In more singular objects, such as stars, $p_{max}/p_0 \to \infty$ as $M \to \infty$. In such a star there is no characteristic p value in the system between p_0 and p_{max}. Thus, $N(p)$ follows a power law between these limits. (The same behavior occurs in higher dimensions for objects with sharp points or edges.) Whenever $N(p)$ shows such power-law behavior, Eqs. (5.2) and (5.3) describe how the moments M_q depend on q. Thus the $D(q)$ exponents, though different from each other, are not independent: the exponents $(q-1)D(q)$ must vary linearly with q for all moments above a certain threshold [cf. Eq. (3.3)]. All moments below this threshold must scale with the same exponent.

Such a hierarchy of scaling exponents is ubiquitous. For example, in the percolation problem the distribution $N(s)$ of cluster masses s has power-law behavior over a range of s which becomes infinite as the critical point is approached. As a result, different moments of the mass distribution scale differently, but the exponents are linear in q (i.e., there is a "constant gap" between successive moments).[17] This linear behavior in q was also hypothesized for DLA fractals.[6] This hypothesis appears to account reasonably for the measured moments M_q for the non-fractal objects studied in this section. A departure from simple linear behavior of the moments seems to occur in DLA, as reported below, and so indicates an interesting difference between a fractal object and a merely singular one like a star. Departure from linear behavior for DLA means that $N(p)$ cannot be described by a simple power-law behavior [see Eq. (4.10)].

VI. COMPUTER MODELS: A-ARM STARS

All of our simulations are based on recently improved models for diffusion-limited aggregation.[18] In these models the particles are allowed to undergo off lattice random walks in which large steps are allowed if the particle

is a long distance from the cluster. This reduces computer time requirements by a factor of about 10^3 and allows simulations to be carried out using a large number ($\simeq 10^6$) of particle trajectories for large (10^3 lattice units or particle diameters) diameter objects. Two versions of the model have been developed.[18] In the off lattice model a particle whose center is x particle diameters away from the center of the closest particle in the aggregate of particles under examination is allowed to move by a distance of up to $x - 2.0$ particle diameters in a randomly selected direction. In the close vicinity of the cluster steps of length 0.7 particle diameters in randomly selected directions take place. If a mobile particle comes in contact with a particle which is part of the cluster at any stage during one of these steps a record is kept of which particle in the cluster was the first to be contacted and a new trajectory is started.

In the semilattice model a similar procedure using off lattice random walks is used,[18] but the object under examination is represented by a set of occupied lattice sites. The particle trajectory stops if the particle (now considered to be of zero diameter) enters an unoccupied lattice site with an occupied nearest neighbor (an unoccupied surface site). A record is kept of how many times each of the unoccupied surface sites is contacted and a new trajectory is started after each contact. At no stage in the simulation is a particle allowed to cross or enter an occupied lattice site. In both models the particle is released from a random position on a circle which just encloses the cluster. The random walk trajectory is terminated if the particle either contacts the object under examination or moves a distance greater than $100 R_{max}$ from the object where R_{max} is its maximum radius.

An A-arm star consists of A linear arms of length L attached at a common point with an angle of $2\pi/A$ between each adjacent pair of arms. In off-lattice simulations, this structure is represented by a single central particle of unit diameter with A arms consisting of $L - 1$ particles whose centers are on the line defining the arm and separated by one diameter. In the semilattice simulations we start with an off-lattice star, and convert the coordinates of the centers of each particle into integers. The lattice sites corresponding to those integers are then filled and the unoccupied surface sites are identified.

The theoretical results given above are unambiguous. Consequently they provide an opportunity to check our computer programs and assess the uncertainties introduced by finite size objects and the use of a finite number of particle trajectories to estimate the harmonic measure. Simulations were carried out for 18-, 12-, and 6-arm stars, as well as simple 2-arm stars ("needles") using both the semilattice and off-lattice models.

Figures 4(a) and 5(a) show some results obtained from the off-lattice model using a 12-arm star with arms 400 particle-diameters long. Figure 4(a) shows the dependence of $\ln[N(R)]$ on $\ln R$, where $N(R)$ is the number of times particles a distance R particle diameters from the origin of the star have been contacted. A total of 10^6 off-lattice trajectories were used to obtain these results. According to Fig. 4(a), $N(R) \sim R^{\omega}$ where the exponent ω has a value $\simeq 5.15$ in good agreement with theory ($\omega = A/2 - 1 = 5$).
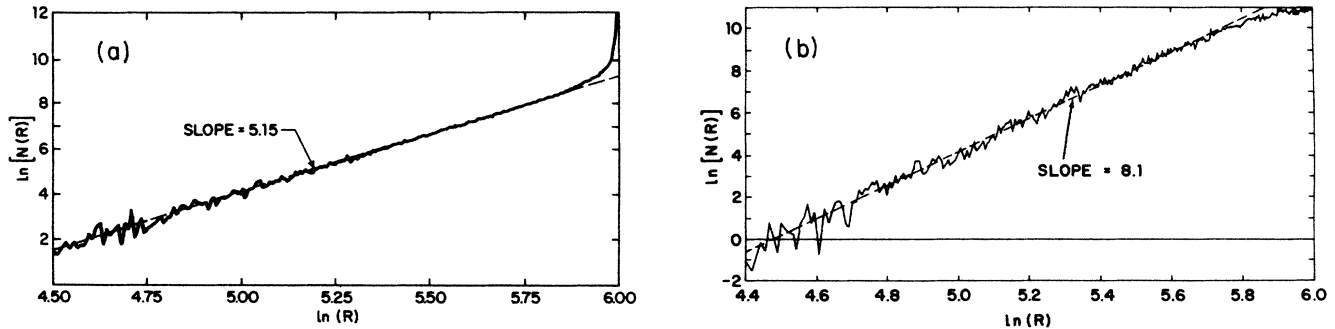
FIG. 4. (a) The number of times $N(R)$ that particles at a distance of R particle diameters from the center of a 12-arm star were contacted during a simulation in which 10^6 particles were used to probe the surface of the star. Each particle trajectory ends as soon as the first contact with the star has been made. Both the star and the particles are assumed to be comprised of circular disks of unit diameter. These results are consistent with theory which indicates that $N(R) \sim R^5$ for small R. (b) The number of contacts for particles located at a distance of $R \pm 0.5$ particle diameters from the center of off-lattice DLA clusters. These results were obtained from simulations using 50 000 particle off-lattice clusters and 5×10^5 random-walk trajectories per cluster.

Figure 5(a) shows the dependence of $\ln[N_\sigma(10^6)]$ on σ, where $N_\sigma(10^6)$ is the number of particles that have been contacted σ times after 10^6 trajectories. These results are consistent with a relationship of the form

$$N_\sigma(\theta) \sim \sigma^\nu , \tag{6.1}$$

where the exponent ν has a value of about $\frac{5}{6}$. Unfortunately, the results of these simulations cannot be used to accurately evaluate the strength of the singularities at the tips of the arms. The reason for this is that the finite size of the particles destroys the singularity.

From the contact probability distribution, an infinite family of surface size measurements can be obtained using the definition of surface size given earlier,

$$\mu_j = \left[\frac{1}{\sum_i p_i^{j+1}} \right]^{1/j} , \tag{6.2}$$

where p_i is the contact probability for particle i in the cluster (or unoccupied surface site in the case of lattice models). Using a 12-arm off-lattice star with arms of length up to 500 diameters and assuming that the quantities μ_i grow with increasing cluster mass M or arm-length

L according to $\mu_j \sim M^{\gamma_j}$ we find $\gamma_1 = 0.882$, $\gamma_2 = 0.727$, $\gamma_3 = 0.651$, $\gamma_4 = 0.611$, $\gamma_5 = 0.587$, $\gamma_6 = 0.570$, $\gamma_7 = 0.559$, and $\gamma_8 = 0.550$ using 10^6 particle trajectories for 15 cluster (star) sizes in the range $M = 601 - 6001$ or $L = 50 - 500$ diameters.

The theory presented above accounts for the powers γ_j. The relation between the $D(q)$ exponents treated theoretically and the γ_j exponents measured in these simulations is given by

$$L^{D(q)} \sim M_q \equiv \left[\sum_j p_i^q \right]^{1/(q-1)} \equiv \mu_j = M^{\gamma_j} ,$$

with $q - 1 = j$ and $M \sim L^D$. Thus

$$D(q)|_{q=j+1} = D\gamma_j .$$

According to (5.3) with $\beta = \frac{1}{2}$, the exponents γ_j should have a value of $0.5(j+1)/j$. Table I compares some of our results for A-arm stars with this prediction. According to our theory the quantities μ_j' defined by $\mu_{j'} = \mu_j^{(i/i+1)}$ should all increase with cluster mass according to $\mu_{j'} M^{0.5}$. Figure 6 shows the dependence of $\ln \mu_j'$ on $\ln M$ for a simulation carried out using off-lattice
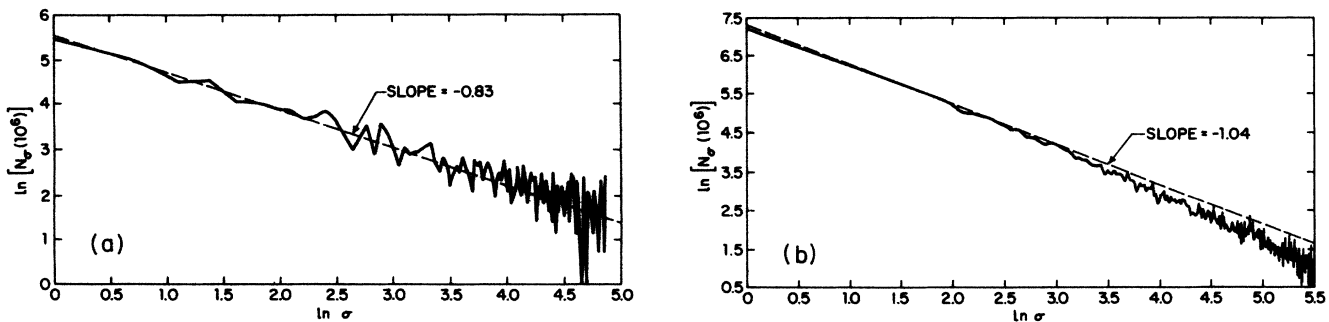
FIG. 5. (a) This figure shows the number of sites $N(\sigma)$ which were contacted exactly σ times during the simulation used to obtain Fig. 4(a). In both figures a star with arms of length 400 particle diameters was used. (b) The number of perimeter sites which have been contacted σ times after 10^6 random-walk trajectories for screened-growth clusters with a fractal dimension of 1.5. The averaged results for five simulations are shown.

TABLE I. Surface mass exponents (γ_i) for A-arm models.

	2 arms/needle S-lattice model 2.5×10^5 traj. $L = 500$	12 arms S-lattice model 2.5×10^5 traj. $L = 500$	12 arms Off-lattice model 2.5×10^5 traj. $L = 500$	2 arms/needle S-lattice model 10^6 traj. $L = 500$	6 arms S-lattice model 10^6 traj. $L = 500$	Theory
γ_1	0.896	0.840	0.883	0.896	0.867	1.0
γ_2	0.735	0.706	0.728	0.735	0.728	0.75
γ_3	0.653	0.637	0.652	0.653	0.655	0.66
γ_4				0.612	0.615	0.625
γ_5				0.587	0.590	0.60
γ_6				0.571	0.574	0.583
γ_7				0.559	0.562	0.571
γ_8				0.552	0.553	0.562

random-walk trajectories at each value of M. Another way of testing our results is to look at the ratio μ'_j/μ'_k for various j and k. According to the theory given above we expect that the ratios should be constant (independent of M, the mass of the star). Figure 7 shows the ratios μ'_j/μ'_k $(j = 1-7, k = 8)$; except for $j = 1$ these ratios are indeed constant to a very good approximation. In general the agreement between the theory presented above and our simulation results are quite good. This agreement is particularly good for the higher "moments" of the contact probability distribution (i.e., for exponents γ_j with j large). The agreement for $j = 1$ does not appear to be very good but we expect logarithmic corrections which could account for most of the apparent disagreement. The higher moments of the contact probability distribution (moments of the harmonic measure) depend only on the singularities in the measure. In the limit of large j, the exponents γ_j converge to a limiting value γ_∞ which describes how the maximum contact probability p_{max} scales with the mass M of the star,

$$p_{max} \sim M^{-\gamma_\infty} . \tag{6.3}$$

In order to assist in the development of a better understanding of the scaling properties of the harmonic measure for fractal objects simulations were carried out for stars in which the number of arms grows with the length of the arms to conform to a mass-length scaling relation-

ship of the form

$$M(L) \sim L^{D'} , \tag{6.4}$$

where $M(L)$ is the mass of a star whose arms are of length L. For all of our simulations the number of arms A is given by

$$A = L^{D'-1} . \tag{6.5}$$

The exponents γ_j defined by Eq. (6.1) and the exponent γ_∞ determined by Eq. (6.3) were obtained using semilattice models. The results of these simulations are shown in Table II. In each case 25 stars with arms of length 60—600 lattice units were probed using 10^6 random-walk trajectories. These stars with a variable number of arms exhibit the "nonclassical" mass length scaling relationship $M(L) \sim L^{D'}$ characteristic of fractals. Because of their simple geometry the nature of the singularities in the harmonic measure at the tips of each of the arms is known. For these objects we would expect that the exponents γ_j should be given by

$$\gamma_j = \frac{(2/D' + j - 1)}{2j} . \tag{6.6}$$

The results shown in Table II seem to be in good agreement with the expression given in Eq. (6.6) particularly for the higher moments (larger values of j).
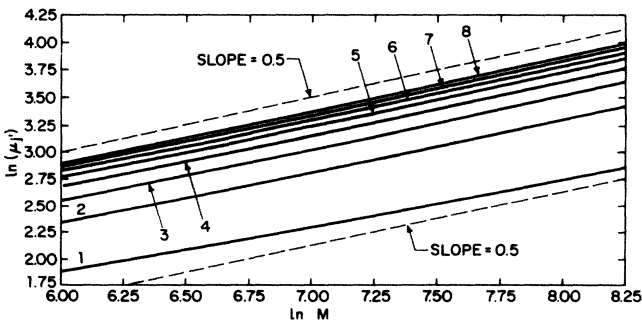
FIG. 6. The dependence of the moments μ'_j (defined in the text) on cluster mass (M) for an off-lattice 12-arm star with arms of length 500 diameters. 10^6 off-lattice random walkers were used to estimate the harmonic measure in the simulation.
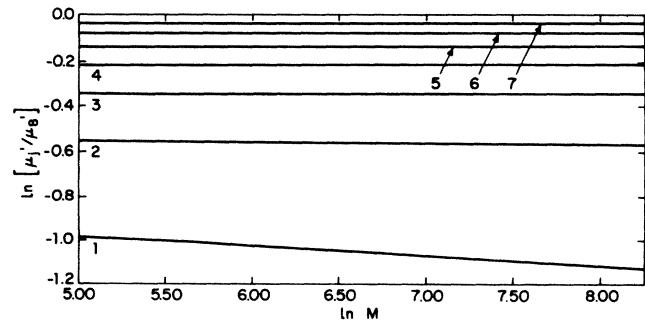

FIG. 7. The dependence of the ratio μ'_j/μ'_8 obtained from the simulation used in Fig. 3. This figure demonstrates that all of the moments μ'_j scale in the same way with increasing cluster mass.

TABLE II. Surface mass exponents γ_i obtained from stars in which the number of arms A is adjusted so that the mass $M(L)$ of stars with arms of length L is given by $M(L) \sim L^{D'}$, i.e., $N(L) \sim L^{D'-1}$.

Exponent	D' 1.33	D' 1.50	D' 1.66
γ_1	0.666	0.624	0.565
γ_2	0.595	0.579	0.540
γ_3	0.562	0.556	0.527
γ_4	0.545	0.543	0.520
γ_5	0.535	0.535	0.515
γ_6	0.529	0.529	0.513
γ_7	0.525	0.524	0.511
γ_8	0.522	0.521	0.510
$\vdots$	$\vdots$	$\vdots$	$\vdots$
γ_∞	0.491	0.492	0.491

VII. COMPUTER MODELS: REGULAR POLYGONS

The same theoretical approach which was used to obtain the surface mass exponents γ_i for the A-arm stars with harmonic measure can be used for regular S-sided polygons as well. A series of simulations was carried out to test the theoretical prediction that the surface mass exponents γ_i should have the value

$$\gamma_i = \min \left\{ \frac{S}{S+2}(1+i^{-1}), 1 \right\} . \tag{7.1}$$

The procedures used were very similar to those described above for the N-arm stars. For the off-lattice simulations the sides of the polygons are represented by a linear string of osculating circles of unit diameter. Each side of the polygon contains $L+1$ such circles, two of which are

TABLE III. A comparison of the surface mass exponents γ_i obtained from off-lattice (o) and semi-lattice (s) computer simulations for the S-sided regular polygons with the theoretical values (t). The asterisk indicates logarithmic corrections.

i	$S=3$ o	$S=3$ s	$S=3$ t	$S=4$ o	$S=4$ s	$S=4$ t
1	1.021	0.964	1.0	1.030	0.993	1.0
2	0.885	0.871	0.9	0.971	0.951	1.0*
3	0.791	0.786	0.8	0.882	0.885	0.889
4	0.741	0.737	0.75	0.828	0.835	0.833
5	0.711	0.707	0.72	0.795	0.803	0.800
6	0.692	0.688	0.7	0.722	0.782	0.778
7	0.678	0.674	0.686	0.757	0.767	0.762
8	0.667	0.664	0.675	0.745	0.756	0.750
∞	0.591	0.587	0.60	0.657	0.684	0.667

i	$S=5$ o	$S=5$ s	$S=5$ t	$S=6$ o	$S=6$ t
1	1.023	0.992	1.0	1.016	1.0
2	1.005	0.974	1.0	1.017	1.0
3	0.939	0.939	0.952	0.979	1.0*
4	0.884	0.901	0.893	0.931	0.938
5	0.849	0.870	0.857	0.895	0.90
6	0.825	0.846	0.833	0.870	0.875
7	0.808	0.829	0.816	0.852	0.857
8	0.796	0.815	0.804	0.839	0.844
∞	0.706	0.704	0.714	0.744	0.75

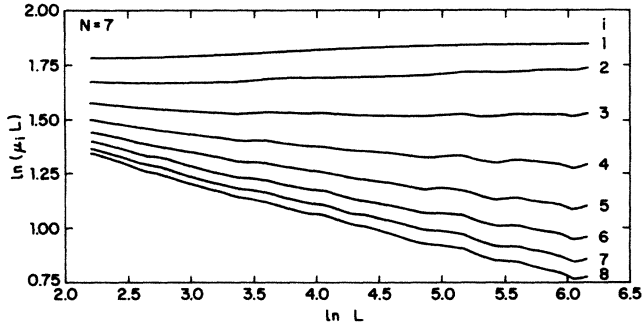| i	$S=7$ o	$S=7$ t	$S=8$ o	$S=8$ t
1	1.012	1.0	1.013	1.0
2	1.019	1.0	1.018	1.0
3	1.001	1.0	1.009	1.0
4	0.962	0.972	0.981	1.0*
5	0.928	0.933	0.949	0.960
6	0.902	0.907	0.923	0.933
7	0.884	0.888	0.904	0.914
8	0.870	0.875	0.889	0.900
∞	0.768	0.778	0.770	0.800

FIG. 8. Dependence of the product $\mu_i L$ on L for off-lattice regular heptagons. The μ_i are surface masses (moments) defined in the text and L is the length of the sides of the heptagon in units of particle diameters.

shared with adjacent sides. Thus a polygon with sides of length L is made up of SL circles of unit diameters. For the semilattice simulations the coordinates of the center of each circle are converted to the nearest pair of integers and the corresponding lattice site is considered to be occupied. For the off-lattice simulations polygons of about 25 different sizes with maximum radii ranging from 5 to 550 particle diameters were used and 5×10^5 random-walk trajectories were used to estimate the harmonic measure. For the semilattice model simulations somewhat larger polygons were used to estimate the harmonic measure (up to 800 diameters maximum radius) and 10^6 random-walk trajectories were used to estimate the harmonic measure for each polygon of about 30 different sizes.

The results of the exponent γ_i obtained from these simulations are shown in Table III. Only the surface masses μ_i for polygons with sides of length L greater than or equal to about 100 diameters were used to obtain the results shown in Table III. Because the regular polygons are not commensurate with the square lattice, better results are obtained for the off-lattice than for the semilattice models. Only results from the off-lattice models are given for $S \geq 6$ in Table III. For $S = 3$, 4, 5, and 6, the results shown in Table III were taken from a single simulation. For $S = 7$ and $S = 8$ the results from two simulations were averaged.

For the $S = 7$ off-lattice case, Fig. 8 shows the dependence of $\ln(L\mu_i)$ on $\ln L$ for $i = 1 - 8$. In the cases where the exponents γ_i are equal to 1 (as is expected for γ_1, γ_2, and γ_3 from the theory) these curves should be horizontal. The results shown in Fig. 8 are consistent with limiting $L \rightarrow \infty$ values of 1.0 for γ_1, γ_2, and γ_3 and values smaller than 1.0 for $\gamma_4 - \gamma_\infty$.

VIII. SCALING PROPERTIES FOR THE HARMONIC MEASURE OF DLA CLUSTERS

2D DLA clusters containing up to 50 000 particles or occupied lattice sites were grown using either the off lattice or semilattice model described above and in earlier work.[18] The surfaces of the clusters were explored using particles following random-walk trajectories. In the case of the off-lattice clusters, a record was kept of how many

times all of the particles in the cluster were contacted. In the case of the semilattice model the number of times each of the unoccupied surface sites was contacted was recorded. At each stage 10^6 random walks were used to estimate the harmonic measure. The results shown in Fig. 6 were obtained from eight such simulations.

Assuming that the ratio $\mu_j^j / \mu_{j+1}^{j+1}$ is related to M by the power-law expression

$$\mu_j^j / \mu_{j+1}^{j+1} \sim M^{-\gamma_j''} , \qquad (8.1)$$

the exponents γ_j'' were obtained by least-squares-fitting straight lines to the dependence of $\ln(\gamma_j^j / \gamma_{j+1}^{j+1})$ on $\ln M$. The results obtained in this fashion were $\gamma_1'' = 0.463 \pm 0.003$, $\gamma_2'' = 0.436 \pm 0.005$, $\gamma_3'' = 0.420 \pm 0.006$, $\gamma_4'' = 0.409 \pm 0.007$, $\gamma_5'' = 0.402 \pm 0.006$, $\gamma_6'' = 0.397 \pm 0.007$, and $\gamma_7'' = 0.394 \pm 0.006$. The exponents γ_n'' are very close to the asymptotic value $\gamma_\infty'' = \gamma_\infty$ but the deviations from this value are quite substantial for the ratios of the lower moments. For DLA γ_∞ should have a value of $(D - 1)/D$ (Refs. 19 and 20), where D (the fractal dimension for DLA) has a value of about 1.7 ($0.7/1.7 = 0.412$). Figure 9 shows the dependence of the ratios on N for simulations carried out using the semilattice model. In each simulation the growth of the cluster was stopped at 24 stages ranging from 10 lattice sites to 50 000 occupied lattice sites.

For the semilattice model the exponent γ_∞ [Eq. (7)] has been measured directly by determining the maximum contact probability p_{max} from 23 simulations each employing 27 clusters in the size range 10–50 000 occupied lattice sites and 10^5 random-walk trajectories for each cluster the results shown in Fig. 10 were obtained. By least-squares-fitting straight lines to the coordinates $(\ln p_{max}, \ln M)$ obtained from each simulation the exponent γ_∞ is estimated to have a value of 0.390 ± 0.004 in good agreement with the results obtained by Turkevich and Scher.[20]

Similar results have been obtained using the off-lattice model. From simulations carried out using 26 cluster masses between 10 particles and 50 000 particles and 250 000 random-walk trajectories for each cluster the results $\gamma_1'' = 0.470 \pm 0.007$, $\gamma_2'' = 0.443 \pm 0.007$, $\gamma_3'' = 0.429 \pm 0.007$, $\gamma_4'' = 0.419 \pm 0.007$, $\gamma_5'' = 0.413 \pm 0.008$, $\gamma_6'' = 0.409 \pm 0.008$, and $\gamma_7'' = 0.406 \pm 0.009$ were obtained.
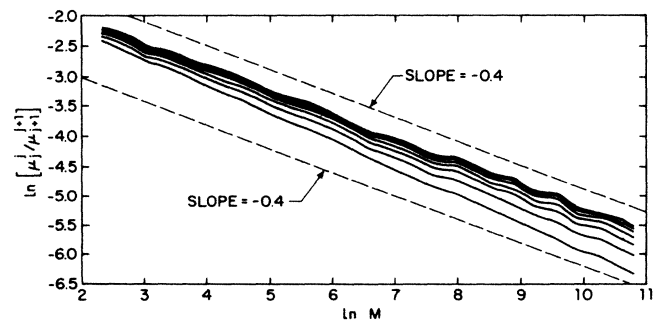

FIG. 9. Dependence of the moment ratio $(\mu_j)^j / (\mu_{j+1})^{j+1}$ for semilattice DLA clusters. These results were obtained from eight simulations using clusters with masses M between 10 and 50 000 occupied sites.
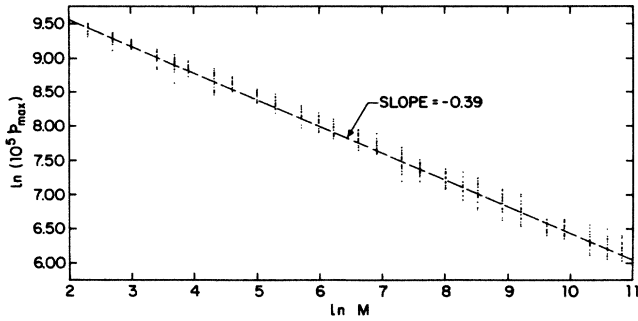
FIG. 10. Dependence of the maximum contact probability p_{max} on cluster mass M for semilattice DLA clusters.

The values obtained for the exponents for γ_n and γ_n'' for both the off-lattice and semilattice DLA models are summarized in Table IV.

The uncertainties given here and elsewhere in this paper represent 95% confidence limits and are the contributions of statistical uncertainties only to the total uncertainty in these exponents. Systematic uncertainties resulting from the finite size of our simulations and the finite number of trajectories are probably larger than the statistical uncertainties.

If the exponents γ_j were linear in j—or, equivalently, $(q-1)/D(q)=q\alpha-f$ with α and f independent of q—we would expect $\gamma_j''=\gamma_\infty$. Our numerical results, Table IV, indicate that γ_j'' deviates slightly from γ_∞ for low moments, indicating therefore that α and f are q dependent. Recently lower moments have been calculated[21] using the electrostatic analogy with DLA giving even stronger evidence of the nonlinearity of $(q-1)/D(q)$ on q and therefore the dependence on q of f and α.

The exponents discussed above provide us with important information concerning the surface of DLA clusters as seen by completely absorbed particles (i.e., by the harmonic measure) and are the relevant quantities for a variety of physically important problems such as catalysis.[22] Figures 2(b)—2(d) show that the measure is concentrated onto perimeter sites at the "tips" of the aggregate; the measure is very small near to the interior of the cluster (i.e., there is strong screening of random walkers). In many ways this measure is similar to that found for the

stars. There seem to be singularities in the measure and the measure is very small for a significant fraction of the sites. Thus Fig. 2 provides a motivation for the description of the harmonic measure for DLA in terms of a fractal set of singularities.

One of the characteristics we would like to know about the harmonic measure is the distribution of the probabilities. The moments μ_i convey some information about this distribution but they are dominated by the sites with the largest contact probabilities p_{max}. Figure 11 shows the results of semilattice simulations in which 10^7 random walkers were used to estimate the harmonic measure for 20 000 site DLA clusters. The averaged results for five such simulations are shown. Figure 11(a) shows the distribution in the number of contacts at various stages during these simulations. Here $N_\sigma(\theta)$ is the number of sites which have been contacted σ times after a total of θ random walkers have been used. Figure 11(b) shows how the number of sites which have been contacted σ times depends on θ for various values of σ. Figure 11 should be compared to Fig. 2 which shows $N_\sigma(\theta)$ for a 12-arm star with large θ.

Similar results have been obtained from simulations of the penetration of random walkers into other fractals. For example, Fig. 5(b) shows the results obtained from five simulations in which 10^6 random walkers were used to estimate the harmonic measure for screened growth clusters[11,12] grown with a fractal dimension of 1.5. These clusters were grown from the center of 1001×1001 lattices until an edge of the lattice was reached by the growth process. Similar results were obtained for the harmonic measure of other fractals, such as screened growth clusters with fractal dimensions of 1.25 and 1.75 and percolation clusters at the percolation threshold $(D=1.89)$. For the $D=1.75$ screened growth fractals clusters containing 18 000 occupied lattice sites were used. The percolation clusters were grown on a square lattice to a size of 75 000—200 000 occupied lattice sites using the methods of Leath[23] and Alexandrowicz[24] assuming a percolation threshold probability p_c of 0.5927.[25] In all cases the distribution of contact probabilities $N_\sigma(\theta)$ for $\theta=10^6$ total contacts can be described approximately by

$$N_\sigma(\theta)\sim\sigma^{-\tau} \qquad (8.2)$$

TABLE IV. The surface mass exponents γ_j and γ_j'' obtained from estimates of the harmonic measure for both semilattice and off-lattice DLA aggregates.

|	Semilattice model		Off-lattice model	
j	γ_j	γ_j''	γ_j	γ_j''
1	0.523±0.005	0.463±0.003	0.529±0.007	0.470±0.007
2	0.493±0.005	0.436±0.005	0.500±0.007	0.443±0.007
3	0.474±0.004	0.420±0.006	0.481±0.007	0.429±0.007
4	0.461±0.005	0.409±0.007	0.468±0.007	0.419±0.007
5	0.450±0.004	0.402±0.006	0.458±0.007	0.413±0.008
6	0.442±0.004	0.379±0.007	0.450±0.007	0.409±0.008
7	0.436±0.004	0.394±0.006	0.444±0.007	0.406±0.009
8	0.431±0.004		0.439±0.007	
⋮	⋮		⋮	
∞	0.390±0.004		0.396±0.009	
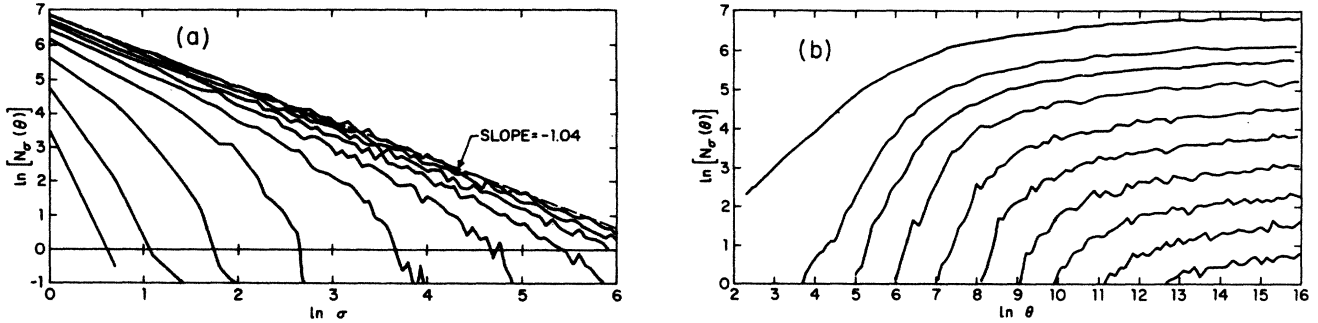
FIG. 11. Distribution of the number of contacts during simulations in which 20 000 site semilattice DLA aggregates were explored using random-walk trajectories with absorbing boundary conditions. (a) shows the contact distribution, where $N_\sigma(\theta)$ is the number of unoccupied surface sites contacted σ times after a total of θ trajectories. Here results are shown for the lowest curve: $\theta = 34$, followed by $\theta = 138$, 549, 2187, 8709, 34 672, 138 034, 549 521, 2 187 674, and 8 709 253. (b) shows how the number of sites contacted σ times after θ particles have been added depends on θ for various fixed values of σ. The lowest curve is $\sigma = 1$, followed by $\sigma = 2$, 3, 5, 10, 19–20, 38–40, 75–80, 150–160, and 299–320. In those cases where a range of σ values $(\sigma_1 - \sigma_2)$ is given results have been averaged for all those sites contacted between σ_1 and σ_2 times inclusively.

for small values of σ. In all cases the effective exponent τ has a value close to one. The results of these simulations are summarized in Table V.

For the case of the off-lattice DLA clusters the harmonic measure was estimated for clusters of different masses. The contact number distribution $N_\sigma(10^6)$ was determined for 23 different cluster sizes in the range $10 \leq M \leq 50\,000$ lattice units. Twenty-nine such simulations were carried out (see Table VI).

Figure 12(a) shows some of the results obtained from the simulations for clusters of size 500, 2000, 5000, 20 000, and 50 000 lattice units.

Using the data for $N_\sigma(\theta) = N(p)$ we have tested the scaling prediction (4.10). From this prediction we have

$$\frac{\ln[n(p)]}{\ln L} = \phi(x) = f\left[q\left[\frac{\ln p}{\ln p_{max}}\right]\right] , \qquad (8.3)$$

plus correction terms of the order of $1/\ln L$. For convenience we have expressed $\ln p_{max}$ and $\ln L$ as functions of $\ln M$ using the following relation:[19,20]

$$\ln p_{max} = -\left[\frac{d_f - 1}{d_f}\right]\ln M , \qquad (8.4)$$

and

$$\ln L = d_f^{-1}\ln M . \qquad (8.5)$$

We have again written $n(p) = pN(p)$ where $n(p)$, as defined in (4.10), is the number of sites with hit probabilities between $\ln p$ and $\ln p + d\ln p$, while $N(p)$ is the number of sites with hit probabilities between p and $p + dp$. Note $N(p)$ is the same, numerically, as $N_\sigma(\theta)$ with $p = \sigma/\theta$.

Figure 12(b) shows the results obtained by scaling $N(p)$ [equivalent to scaling $N_\sigma(\theta)$ using Eq. (8.3)]. It should be noted that the scaled probability distribution functions intersect the x axis at $-\gamma_\infty$ and have a maximum value of about 1.0 as is expected[7,26] from (4.2) and (4.4). The scaling collapse is not particularly good but is clearly improving as the cluster mass increases. Consequently we conclude that our results are consistent with (4.5). A better way to obtain the function f in (8.3) and therefore the data collapse would have been to extrapolate $\ln[n(p)]/\ln L$ as a function of $1/\ln L$. In this way one could get rid of the $1/\ln L$ correction terms.

It should be noted that for DLA (unlike the screened-growth clusters[26]) we cannot determine the small parts of the growth probability measure and consequently only obtain part of the function $f[q(x)]$. The fact that $f[q(x)]$ for the harmonic measure of DLA clusters (and other fractals) has a quite flat region near its maximum value can be related to the fact that (8.2) is approximately

TABLE V. Effective values for the exponent τ which describes the contact distribution $N_\sigma(\theta)$ after $\theta = 10^6$ random-walk trajectories have been used to estimate the harmonic wave size for various random fractals. The exponent τ was obtained by least-squares-fitting straight lines to the coordinates $(\ln N_\sigma(10^6), \ln\sigma)$ for the sites which had contact numbers σ in the range $\sigma_1 \leq \sigma \leq \sigma_2$.

Model	D	$\sigma_1 = 3, \sigma_2 = 30$	τ $\sigma_1 = 5, \sigma_2 = 25$	$\sigma_1 = 10, \sigma_2 = 100$
Screened growth	1.25	0.91±0.18	0.94±0.21	1.13±0.14
Screened growth	1.5	1.10±0.03	1.11±0.07	1.24±0.06
Screened growth	1.75	1.043±0.03	1.034±0.04	1.165±0.03
Percolation	≃1.89	0.881±0.028	0.865±0.030	0.951±0.030
	(1.75 hull)			
DLA	≃1.70	1.174±0.018	1.166±0.026	1.24±0.06

TABLE VI. Values of the exponents $\gamma_1 - \gamma_8$ and γ_∞ estimated by probing the surfaces of screened-growth clusters with random-walk trajectories. For each value of the fractal dimension 250 000 random walks were used to estimate the harmonic measure for six different clusters at about 20 stages during their growth.

Surface size	Fractal dimension		
Exponent	1.25	1.50	1.75
γ_1	0.677±0.016	0.591±0.005	0.517±0.003
γ_2	0.619±0.015	0.547±0.004	0.488±0.003
γ_3	0.582±0.015	0.519±0.005	0.470±0.003
γ_4	0.557±0.016	0.499±0.005	0.458±0.003
γ_5	0.539±0.017	0.485±0.005	0.448±0.003
γ_6	0.526±0.019	0.474±0.005	0.440±0.003
γ_7	0.516±0.020	0.466±0.005	0.434±0.003
γ_8	0.508±0.020	0.459±0.006	0.429±0.004
$\vdots$	$\vdots$	$\vdots$	$\vdots$
γ_∞	0.449±0.022	0.407±0.011	0.387±0.007

correct and that the effective exponent τ has a value close to 1.0 (Table V).

The scaling relation (8.3) has recently[26] been confirmed also for the screened-growth model,[11-13] for which exact knowledge of the growth probabilities allowed a better test. We have also checked for DLA whether we could exclude a conventional scaling relation such as

$$N_\sigma(\theta,M) \sim M^\alpha f_\theta(\sigma M^\beta) , \qquad (8.6)$$

where $N_\sigma(\theta,M)$ is the number of sites that have been hit σ times in a simulation carried out using a cluster of mass M with θ random-walk trajectories. Attempts to collapse the curves $N_\sigma(\theta,M)$ for clusters of different mass M onto a single curve using $\alpha \simeq 1.0$ and $\beta = \gamma_{max} \simeq 0.4$ were not successful.

Simulations have also been carried out to measure the number of contacts $N(R)dR$ at a distance of $R \pm dR/2$ from the seed or origin of the DLA aggregate. Off-lattice DLA clusters of 50 000 particles were generated and their harmonic measure was estimated using 5×10^5 off-lattice random walkers. Figure 4(b) shows the dependence of $N(R)$ on R obtained from these simulations. This figure indicates that $N(R)$ has an approximate power-law

dependence on R

$$N(R) \sim R^\delta . \qquad (8.7)$$

The exponent δ has a value of 8.3 ± 0.6 for distances, R, in the range $100 \leq R \leq 300$ particle diameters from the growth site or seed. In this regard the distribution of contact probabilities inside a DLA aggregate is similar to that found in a star with 14 or 15 arms.

To explore the contact probability distribution further 170 semilattice 2D DLA clusters were grown to a mass of 50 000 occupied lattice sites and 10^6 random walkers were used to estimate the harmonic measure for each cluster. Figure 13 shows the results obtained for the contact number of the unoccupied surface sites in each cluster normalized by the maximum contact number for each cluster. Here $NT_\sigma(\theta)$ is the number of sites which have been contacted σ or more times after θ random-walk trajectories.

The surface mass exponents γ_n have been determined for 2D percolation clusters by probing the surface of growing percolation clusters[23,24] using random walkers. Percolation clusters were grown to a size greater than or equal to 10^5 occupied lattice sites on a square lattice and the harmonic measure was estimated at about 30 stages during the growth process (for clusters in the size range $10-10^5$ occupied lattice sites) using 10^5 random-walk probes at each stage. From 30 such simulations the values of the exponents γ_n were found to be $\gamma_1 = 0.483 \pm 0.005$, $\gamma_2 = 0.460 \pm 0.005$, $\gamma_3 = 0.445 \pm 0.006$, $\gamma_4 = 0.434 \pm 0.006$, $\gamma_5 = 0.425 \pm 0.006$, $\gamma_6 = 0.419 \pm 0.006$, $\gamma_7 = 0.413 \pm 0.006$, $\gamma_8 = 0.409 \pm 0.007$, and $\gamma_\infty = 0.372$.

For both percolation clusters and DLA aggregates the dimensions $D(q)$ that describe the harmonic measure have also been estimated using the box counting method.[6,27] Table VII compares the quantities D_q and $D\gamma_j$ for percolation clusters, semilattice DLA and off-lattice DLA. Except for the case $q=2$, $j=1$ our results support the idea that $D_q = D\gamma_j$ for $q = j + 1$. Our method of estimating the harmonic measure gives relatively good results for the values of the measure where the measure is large but poor results in those regions where the measure is small. Consequently we expect our results to be most accurate for large q or j. The relatively poor agreement for small q or j is probably a consequence of our inability to deter-
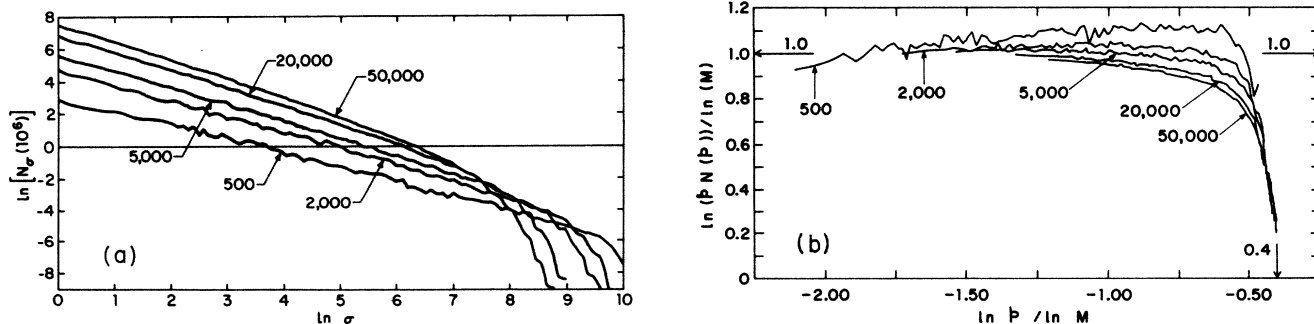

FIG. 12. (a) The distributions in the number of contact probabilities σ for semilattice DLA clusters with masses of 500, 2000, 5000, 20 000, and 50 000 occupied lattice sites. The results for 11 simulations, each employing 10^6 random-walk trajectories per cluster, are shown. (b) The site contact number distributions $N_\sigma(10^6,M)$ shown in (a) have been used to obtain the contact probability distribution $n(p) = pN(p)$ which have been plotted to exhibit the scaling form given in Eq. (8.3).
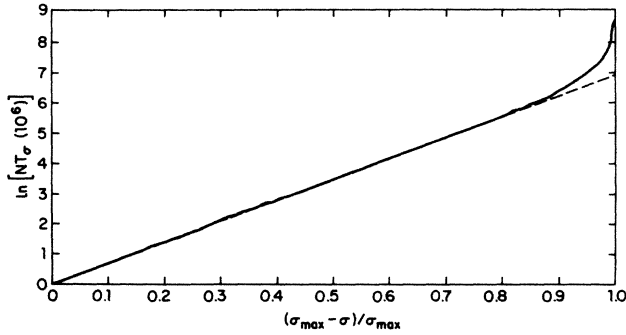
FIG. 13. The number of perimeter sites contacted σ or more times, $NT_\sigma(\theta)$, as a function of $(\sigma_{max}-\sigma)/\sigma_{max}$. These results were obtained from 170 simulations using 50 000 site off lattice DLA clusters and $\theta = 10^6$ trajectories per cluster. σ_{max} and $(\sigma_{max}-\sigma)/\sigma_{max}$ were determined separately for each cluster before the results were averaged.

mine the value of the harmonic measure in those regions where the measure is small (the strongly screened interior regions of the cluster).

In our earlier work the exponents γ_1, γ_2, and γ_3 which describe how the effective surface masses M_1, M_2, and M_3 as seen by random-walk probes, increase with increasing cluster mass were determined for several screened growth clusters with fractal dimensions of 1.25, 1.5, and 1.75. In this work 25 000 random-walk trajectories were used to estimate the harmonic measure for six clusters at each of the three fractal dimensions. Using the same 18 screened growth clusters these exponents have been redetermined using 250 000 random-walk trajectories

and/or clusters and the range of exponents has been extended up to γ_8. The exponent γ_{max} has also been determined from the maximum number of contacts at each cluster size. The results shown in Table IV are in good agreement with our earlier work.

IX. THE OCCUPATION PROBABILITY MEASURE FOR SCREENED-GROWTH FRACTALS

In the case of the DLA model the harmonic measure is equivalent to the measure defined by the growth probabilities for the fractals (i.e., the occupation probability measure). In other cases these two measures are not equivalent. For the case of clusters grown using the screened growth model[11-13] (a model for which the fractal dimension is known exactly) the occupation probability measure has been estimated from the computer simulations in which clusters with fractal dimensions of $\frac{4}{3}$ and $\frac{5}{3}$ were generated on 1001×1001 square lattices (see Fig. 14). A family of "moments" μ_j can be defined for this measure in the same way that the moments μ_j were defined for the harmonic measure,

$$\mu_j = \left[\frac{1}{\sum_i p_i^{j+1}} \right]^{1/j} . \tag{9.1}$$

Here the probabilities p_i are the growth probabilities for the ith unoccupied surface site (growth site). We have determined the dependence of the moments μ_j on the cluster mass M. From simulations carried out for the case $D = \frac{4}{3}$ and formulations carried out using screened growth clusters with a fractal dimension of $\frac{5}{3}$, we find

TABLE VII. A comparison of the exponents D_q and $D\gamma_j$ for the harmonic measure of 2D percolation clusters and both off-lattice and semilattice DLA aggregates.

Exponent	Percolation clusters $p_c = 0.5927$ $D = 1.89$		Off-lattice DLA $(D = 1.71)$	
	D_q	$D\gamma_j$	D_q	$D\gamma_j$
$j = 1, q = 2$	1.017 ± 0.009	0.913 ± 0.009	0.980 ± 0.010	0.905 ± 0.012
$j = 2, q = 3$	0.947 ± 0.008	0.869 ± 0.009	0.856 ± 0.005	0.855 ± 0.012
$j = 3, q = 4$	0.886 ± 0.013	0.841 ± 0.011	0.810 ± 0.006	0.823 ± 0.012
$j = 4, q = 5$	0.869 ± 0.018	0.820 ± 0.011	0.782 ± 0.006	0.800 ± 0.012
$j = 5, q = 6$	0.848 ± 0.024	0.803 ± 0.011	0.763 ± 0.008	0.783 ± 0.012
$j = 6, q = 7$	0.835 ± 0.029	0.792 ± 0.011	0.754 ± 0.010	0.770 ± 0.012
$j = 7, q = 8$	0.825 ± 0.036	0.781 ± 0.011	0.748 ± 0.012	0.780 ± 0.012
$j = 8$		0.773 ± 0.011		0.751 ± 0.012
$j = \infty$		0.703 ± 0.011	0.71	0.677 ± 0.015

Semilattice DLA $(D = 1.70)$	D_q	$D\gamma_j$
γ_1	0.973 ± 0.003	0.889 ± 0.009
γ_2	0.875 ± 0.006	0.838 ± 0.009
γ_3	0.837 ± 0.007	0.806 ± 0.007
γ_4	0.811 ± 0.008	0.784 ± 0.009
γ_5	0.791 ± 0.009	0.765 ± 0.007
γ_6	0.775 ± 0.010	0.751 ± 0.007
γ_7	0.761 ± 0.011	0.741 ± 0.007
γ_8		0.732 ± 0.007
γ_∞		0.663 ± 0.007

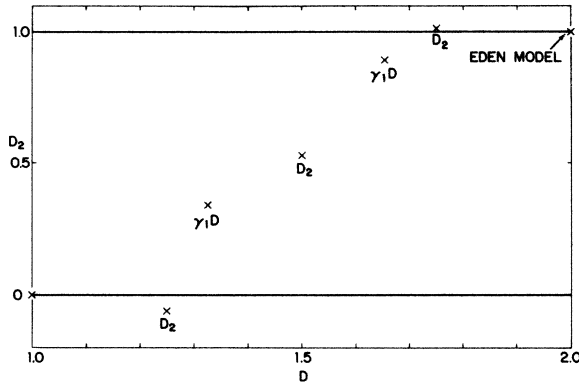SCALING PROPERTIES FOR THE SURFACES OF FRACTAL . . .

FIG. 14. Correlation dimensions D_γ for screened growth clusters with various fractal dimensions. For $D = \frac{4}{3}$ and $D = \frac{5}{3}$, D_2 was obtained from the relation $D_2 = \gamma_1 D$. For $D \to 2$ [the Eden model (Ref. 28)] $D_2 = 2$, $\gamma_1 = 1$ and for $D \to 1$, $D_2 = \gamma_1 = 0$.

TABLE VIII. Values for the exponents $\gamma_1 - \gamma_8$ and γ_∞ which indicate how the surface masses $\mu_1 - \mu_8$ and $1/p_{max}$ increase with increasing cluster size for screened-growth clusters with fractal dimensions of $\frac{4}{3}$ and $\frac{5}{8}$. The surface masses are defined by the growth probability measure. For the $D = \frac{4}{3}$ clusters the results from 60 simulations were used and for $D = \frac{5}{3}$. 32 simulations were used.

Exponent	$D = \frac{4}{3}$	$D = \frac{5}{3}$
γ_1	0.253 ± 0.047	0.539 ± 0.007
γ_2	0.210 ± 0.045	0.482 ± 0.009
γ_3	0.191 ± 0.043	0.450 ± 0.009
γ_4	0.180 ± 0.041	0.429 ± 0.010
γ_5	0.174 ± 0.041	0.416 ± 0.010
γ_6	0.169 ± 0.040	0.406 ± 0.010
γ_7	0.166 ± 0.039	0.397 ± 0.010
γ_8	0.164 ± 0.038	0.393 ± 0.010
$\vdots$	$\vdots$	$\vdots$
γ_∞	0.138 ± 0.041	0.347 ± 0.009

power-law relationships between the moments μ_j and M (the cluster mass)

$$\mu_j \sim M^{\gamma_j} . \tag{9.2}$$

Effective values for the exponents γ_j are given in Table VIII. In the course of some earlier work the density-density correlation functions were measured for the active zone (occupation probability measure) of screened-growth clusters with fractal dimensions of 1.25, 1.50, and 1.75. In all cases the correlation function $C^a(r)$ was found to have the form

$$C^a(r) \sim r^{-y} \tag{9.3}$$

for distances larger than a few lattice units and smaller than the overall size of the cluster. The exponents y were found to have values of about 2.05, 1.45, and 1.00, respectively, for $D = 1.25$, 1.50, and 1.75.

X. SUMMARY

We have investigated the distribution of hit probabilities near the surface of a variety of fractal and nonfractal objects. The moments of this distribution for both fractal and nonfractal objects are characterized by an infinite set of exponents. In the case of nonfractal objects (needle, polygon, stars), the hit distribution is characterized by a power law. As a consequence the infinite set of exponents

are not independent but have a linear dependence in q. In the case of fractal objects like DLA, screened-growth models, or percolation clusters the moments seem to deviate from such a simple linear law. This has the consequence that $n(p)$ is described by (4.10) and not by a simple power law.

This departure from a simple power-law behavior has recently been found in the voltage distribution that arises when a current is passed through a percolation at the percolation threshold.[5,16] The hit probability and the voltage distribution in fact are very similar: the hit distribution can be related to the density of the random walkers on the surface of the cluster, and the density can be obtained by calculating the voltage drop on the surface sites assuming that the aggregate is a conductor of constant potential. Therefore this distribution is related to the voltage distribution on the surface fractal.

ACKNOWLEDGMENTS

---

*Present address: Central Research and Development Department, E. I. DuPont de Nemours and Company, Wilmington, Delaware 19898.

†Gruppo Nazionale di Struttura Della Materia, Dipartimento di Fisica, Universita' di Napoli, Mostra d'Oltremare, Pad. 19 80125 Napoli, Italy.

[1]A. Coniglio and H. E. Stanley, Phys. Rev. Lett. 52, 1068 (1984).

[2]P. Meakin, H. E. Stanley, A. Coniglio, and T. A. Witten, Phys. Rev. A 32, 2364 (1985).

[3]B. B. Mandelbrot, The Fractal Geometry of Nature (Freeman,

San Francisco, 1982) and references therein.

[4]The classic papers on exponent hierarchies are B. B. Mandelbrot, J. Fluid Mech. 62, 331 (1974), and H. G. E. Hentschel and I. Procaccia, Physica D 84, 440 (1983).

[5]L. de Arcangelis, S. Redner, and A. Coniglio, Phys. Rev. B 31, 4725 (1985).

[6]T. C. Halsey, P. Meakin, and I. Procaccia, Phys. Rev. Lett. 56, 854 (1986).

[7]T. C. Halsey, M. H. Jensen, L. P. Kadanoff, I. Procaccia, and B. Shraiman, Phys. Rev. A 33, 1141 (1986).

[8]An introduction and review of the early work (Refs. 2–7) on

an "infinite hierarchy of exponents" is contained in the 1985 Cargèse lectures of A. Coniglio, in *On Growth and Form: Fractal and Nonfractal Patterns in Physics,* edited by H. E. Stanley and N. Ostrowsly (Nijhoff, Dordrecht, 1985), p. 101.

[9]T. A. Witten and L. M. Sander, Phys. Rev. Lett. **47**, 1400 (1981).

[10]T. A. Witten and L. M. Sander, Phys. Rev. B **27**, 5686 (1983).

[11]P. A. Rikvold, Phys. Rev. A **26**, 674 (1982).

[12]P. Meakin, Phys. Rev. B **28**, 6718 (1983).

[13]P. Meakin, F. Leyvraz, and H. E. Stanley, Phys. Rev. A **32**, 1195 (1985).

[14]P. Meakin and T. A. Witten, Phys. Rev. A **28**, 2985 (1983).

[15]A. preliminary account of this scaling was presented by A. Coniglio, in *Conference on Fractals in Physics, Trieste, Italy, 1985,* edited by Pietronero and E. Tosatti (North-Holland, Amsterdam, 1986).

[16]L. de Arcangelis, S. Redner, and A. Coniglio, Phys. Rev. B (to be published).

[17]D. Stauffer, Phys. Rep. **54**, 1 (1979).

[18]P. Meakin, 1985 Cargèse lectures (Ref. 8); J. Phys. A **18**, L661 (1985).

[19]F. Leyvraz, J. Phys. A **18**, L941 (1985).

[20]L. Turkevich and H. Scher, Phys. Rev. Lett. **55**, 1026 (1985).

[21]C. Amitrano, A. Coniglio, and F. di Liberto, Phys. Rev. Lett. **57**, 1016 (1986).

[22]P. Meakin, Chem. Phys. Lett. **123**, 428 (1986).

[23]P. L. Leath, Phys. Rev. B **14**, 5046 (1976).

[24]F. Alexandrowicz, Phys. Lett. **80A**, 284 (1980).

[25]H. E. Stanley, P. J. Reynolds, S. Redner, and F. Family in *Real Space Renormalization,* edited by T. W. Burkhardt and J. M. J. Van Leuween (Springer-Verlag, Berlin, 1982), Vol. 30, Chap. 7.

[26]P. Meakin, Phys. Rev. A **34**, 710 (1986).

[27]T. C. Halsey, P. Meakin, and I. Procaccia, Phys. Rev. Lett. **56**, 854 (1986).

[28]M. Eden, in *Fourth Berkeley Symposium on Mathematics, Statistics and Probability,* edited by J. Neeyman (University of California Press, Berkeley, 1961).